JMEPEG (2007) 16:30–34
DOI: 10.1007/s11665-006-9004-0

1059-9495/$19.00

The Effect of Surface Engineering Treatments on the Fatigue Behavior of 2024-T351 Aluminum Alloy

C.A. Rodopoulos, A.Th. Kermanidis, E. Statnikov, V. Vityazev, and O. Korolkov

(Submitted March 23, 2006)

The work examines the effect of controlled shot peening (CSP), laser shock peening (LSP) and ultrasonic impact treatment (UIT) on the fatigue behavior of 2024-T351 aluminum alloy. The testing methodology has been designed to extract information regarding specific products of the treatments and their individual affect on fatigue damage. The work concludes that all three surface treatments improve the fatigue resistance of the material with the LSP covering the areas of safe-life and damage tolerance, the control shot peening can only benefit the area of short crack growth while the UIT proved to benefit both the short and long crack growth.

Keywords aerospace, mechanical testing, surface engineering

1. Introduction

Surface engineering treatments or SETs (the reader might also come along a different name that of Engineering Mechanical treatments) have been primarily developed in order to increase the fatigue resistance of engineering components. There are more than six known and commercially available SETs. Despite the fact that in many works they have been classified under the same header, the true distinction can only be appreciated in relation to the strain rate they induced on the surface. Low plasticity burnishing and deep rolling belong to the low-medium strain rate group ($<10^2$ s^{-1}). Shot peening and laser shock peening (LSP) belong to intermediate strain rate group (10^3 s^{-1}–10^5 s^{-1}). Explosive hardening and ultrasonic impact treatment (UIT) belong to high strain rate group ($>10^5$ s^{-1}) (Ref 1-2). The latter group can also be classified within the severe plastic deformation processes along with Equal Channel Angular Extrusion (Ref 3) and Accumulative Roll Bonding (Ref 4) due to its ability to produce near surface nanocrystalline state (grain size typically less than 100 nm) (Ref 5).

The assortment of possible microstructures obtained by SETs can be relatively broad with strong dependency on the process parameters and the material in question. However, enhanced near-surface dislocation densities are actively present in all six cases and show a variety of arrangements, from homogeneous distribution in tangles to cell-formation (Ref 6, 7). Wavy slip materials subjected to low and medium strain rates are likely to exhibit cell-like dislocation arrangements. Planar slip materials on the other hand, when subjected to high strain rates formed tangled dislocations (Ref 2).

Cold work, residual stresses, microstructure, stability of residual stresses under cyclic loading, surface roughness and the hardness of the target material can all affect the fatigue behavior of materials. Yet, they are likely to affect different fatigue stages, see Table 1. It is, therefore, difficult to classify the performance of SETs by conducting simple *S-N* curves and a more rigorous testing methodology is required. The above comes as a result to the fact that Stage I (short) and Stage II (long) crack growth are likely to affect different portions of the total number of failure. For example, Stage I crack growth is likely to significantly affect the area of high cycle fatigue while Stage II crack growth will dominate the area of low cycle fatigue. Of course, the presence and size of Stage I cracking depends on the material in question and on the testing conditions. In general, materials exhibiting low values of σ_{fl}/σ_y^c are more likely to exhibit short cracking when tested at low positive stress ratios (Ref 8). The crack shape in relation to the setup testing geometries should also be considered since values of less than the unity will promote such behavior.

In this work, the authors investigate and report on the effect of three SETs belonging in the intermediate (controlled shot peening [CSP] and laser shock peening [LSP]) and high strain rate group (UIT) on the fatigue behavior of the popular 2024-T351 aluminum alloy. The material and the testing conditions used have been selected in order to promote short cracking.

Table 1 Effect of SET products on fatigue loading (Ref 9)

SET product	Stage I crack growth	Stage II crack growth
Surface roughness	Accelerates	No effect
Residual compressive Stresses	No effect	Retards
Stability of residual stresses	No effect	Retards
High dislocation density	Retards	No effect
Cold work/strain hardening	Retards	Accelerates

C.A. Rodopoulos, Structural Materials and Integrity Research Centre, Materials & Engineering Research Institute, Sheffield Hallam University, City Campus, Howard Street, Sheffield S1 1WB, UK; **A.Th. Kermanidis,** Laboratory of Technology and Strength of Materials, Department of Mechanical Engineering & Aeronautics, University of Patras, Patras 26 500, Greece; **E. Statnikov,** Applied Ultrasonics, ?871 Old Leeds Rd, Irondale, AL 35210, USA; and **V. Vityazev** and **O. Korolkov,** Northern Scientific Technological Company, 6 Voronin str., Severodvinsk, Arkhangelsk Region 164500, Russian Federation. Contact e-mail: C.Rodopoulos@shu.ac.uk.

2. Experimental Conditions – Set Evaluation

The material used in this work was rolled 2024-T351 Al alloy plate provided by Airbus UK and manufactured by Alcoa. The material has a chemical composition as shown in Table 2. The mechanical properties of the material perpendicular to the rolling direction (LT) have been obtained according to ASTM E8m-94a and are shown in Table 3. The material has a pancake shape grain structure with an average grain size of 220 μm, 80 μm and 52 μm in the longitudinal, transverse and thickness direction.

Controlled shot peening was performed using a Tealgate peening machine. The peening intensity was 4 A and it was achieved using a S110 (diameter 0.279 mm and hardness 410.5-548.5 Hv) spherical cast steel shot, incidence angle of 90° and a coverage rate of 100%. These conditions were recommended in (Ref 10) where a study of maximum, near surface, residual stress profile to counterbalance the increased surface roughness profile was made. Laser shock peening was performed in water confinement using a Continuum YAG Laser (Powerlite plus) operating in the green wavelength (0.532 μm) regime. The output energy was approximately 1.3 J with pulse duration in the 6-7 ns regime. All specimens were protected from the thermal effects of LSP by a 70 μm aluminum coating. The laser intensity was set to 10 GW/cm^2 (estimated pressure of 5 GPa) with a focal point of 2 mm. The specimens were treated using an overlapping rate of 50% (1 pass = 4 local pulses) and charged with three passes. The selected parameters have been previously verified (Ref 11). The UIT was performed using a carrier frequency of 36 KHz, pin diameter of 5 mm, amplitude under load of 18 μm, impact frequency of 260 Hz and pressure of 3 kg.

Residual stress measurements on all three cases were conducted on Philips Xpert Pro XRD using Cr-*K*a-radiation. Depth profiles were taken using sequential electrochemical polishing. The residual stresses were calculated using the $\sin^2\psi$ method. Figure 1 shows the residual stress profiles from all three cases. The results indicate that all three SETs delivered a similar near-surface residuals stress magnitude of ~220 MPa. LSP and CSP exhibited higher and more uniform residual stress profile in the region between 100 and 300 μm, while the UIT dominates the region between 0.4 and 1.1 mm. In terms of maximum depth LSP and UIT demonstrated penetration depth as much as 1.6 mm (considering an XRD error of 40 MPa) compared to 1.1 mm delivered by the CSP.

Microhardness testing was performed to provide an indication of the amount of strain hardening induced by the three processes. All measurements were taken across the thickness of the coupons after diamond saw slicing. A load of 500 g (to minimize volumetric effects from the Cu precipitate) was selected on a Mitutoyo MVK H1 microhardness tester. The results are shown in Fig. 2.

The results indicate that both the CSP and UIT induced significant strain hardening in contrast to LSP, which indicates negligible effect. The UIT shows a significant deeper penetration depth compared to the CSP. Close examination at the near surface measurements (<170 μm) reveals that the UIT exhibits peak value at around 150 μm while its performance close to the surface is rather poor compared to CSP.

Surface roughness measurements were undertaken using a Mitutoyo Stylus profilometer. The results are shown in Table 4. The results indicate that all three SETs increased the surface

Table 2 Chemical composition of 2024-T351 in wt.%

Alloy		Si	Fe	Cu	Mn	Mg	Cr	Zn	Ti	Zr	Al
2024-T351	Min	–	–	3.8	0.30	1.2	–	–	–	–	Balance
	Max	0.50	0.50	4.9	0.90	1.8	0.10	0.25	0.15	–	

Table 3 Basic mechanical properties of 2024-T351 according to ASTM E8m-94a

Mechanical properties	Mean	99% Conf.	SD	SE
0.2% Yield strength (MPa)	347.4	5.1	4.5	1.5
Tensile strength (MPa)	504.6	2.6	2.3	0.7
Cyclic yield stress (MPa)	487.2	2.5	2.4	1.1
Elongation (%)	15.0	0.2	0.2	0.07
Fracture toughness—plane stress [MPam$^{1/2}$] for thickness 1.6 mm	135.5	8.7	3.0	1.5
Strain energy density (MJ/m^3)	70.5	0.6	0.5	0.2

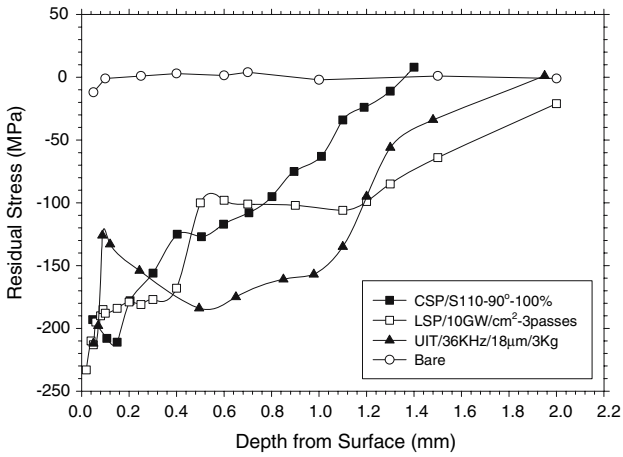

Fig. 1 Residual stress profiles for the three selected SETs on 2024-T351 taken from a 5 mm coupon. Measurements from the bare material are reported for comparison

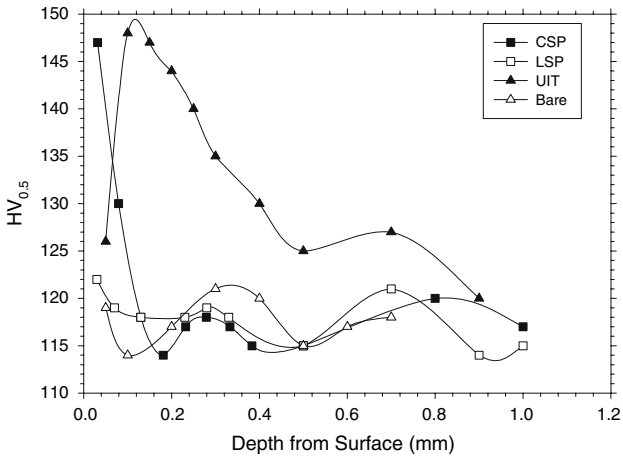

Fig. 2 Through thickness microhardness for the three selected SETs on 2024-T351. Each point is averaged out of five measurements

roughness. Considering that surface roughness in the form of micronotches is uniformly distributed along the surface area, the elastic stress concentration can be calculated as (Ref 12),

$$K_t = 1 + 1.05\left(\frac{R_t}{S}\right) \quad \text{(Eq 1)}$$

where the parameters R_t and S are, respectively, the mean of peak-to-valley heights and the mean spacing of adjacent peaks in the surface roughness profile. The results from Eq (1) are also shown in Table 4. Yet, for proper comparison against the surface quality of the bare material, relative values ($\overline{K_t}$) should be used. The results indicate that CSP increased the relative roughness by 18%, the LSP by 7% and the UIT by 8%.

3. Experimental Conditions—Cyclic Testing

Fatigue testing was performed in a four-point bending configuration to investigate the effect of a stress gradient and to minimize the possibility of subsurface cracking. Test-pieces were cut parallel to the rolling direction. Test-piece dimensions are shown in Fig. 3. The stress gradient is given by the linear relationship $\sigma/\sigma_{max} = 0.36z$, where z is the position of the bending fiber from the neutral/central fiber. Only the top surface was treated by SETs. The testing setup and material promotes the propagation of short crack growth in the form of corner cracking, making it an ideal configuration to examine the potential of cold work.

The experiments were conducted at room temperature using a sinusoidal waveform, at a frequency of 15 Hz and a stress ratio (minimum to maximum stress ratio) of $R = 0.1$. Fatigue data in the form of *S-N* curves are shown in Fig. 4.

The results indicate that all three SETs improved the fatigue life of the material. In particular, LSP exhibited significant improvement compared to both in the low and high cycle fatigue region. CSP showed the smallest improvement although consistent in both fatigue regions. Finally the UIT demonstrated improvement comparable to LSP in the low cycle fatigue region, while beyond the 300 K cycles mark the improvement resembled that of CSP. As indicated above comparison of SETs having different surface roughness conditions under nominal maximum stress levels can easily misguide the investigation especially when the understanding of the parameters controlling life improvement is in question. It is, however, important to note that such representation is only applicable in the case of bending loading where σ_{max} denotes the surface stress. Figure 5 shows all the data from Fig. 4 against the relative maximum stress.

Herein the results indicate that in the rear of low cycle fatigue all three SETs demonstrated similar improvement of fatigue life. In the high cycle fatigue region, UIT seems to follow in performance both the CSP and LSP. Of particular importance is the fact that in terms of stress level, the LSP switched the behavior of the bare material from low to high cycle fatigue (the 300 MPa fatigue limit corresponds to 100 K cycles in the bare).

The above results strongly contradict Table 1. In the case of LSP in particular, with negligible cold work and hence small potential in improving the high cycle fatigue region, the results indicate that it outperformed both the CSP and the UIT process

Table 4 Surface roughness profiles from the three selected SETs and bare material along with the corresponding induced elastic stress concentration and its relative value

Condition	Ra, μm	Rtm, μm	*S*, mm	K_t	$\overline{K_t}$
Bare	2.11	5.6	0.052	1.11	1
CSP	4.70	38.1	0.124	1.32	1.18
LSP	4.21	34.4	0.188	1.19	1.07
UIT	4.52	36.2	0.191	1.20	1.08

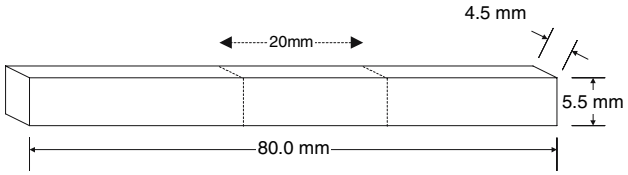

Fig. 3 Test-piece dimensions. The dotted lines represent the gauge area

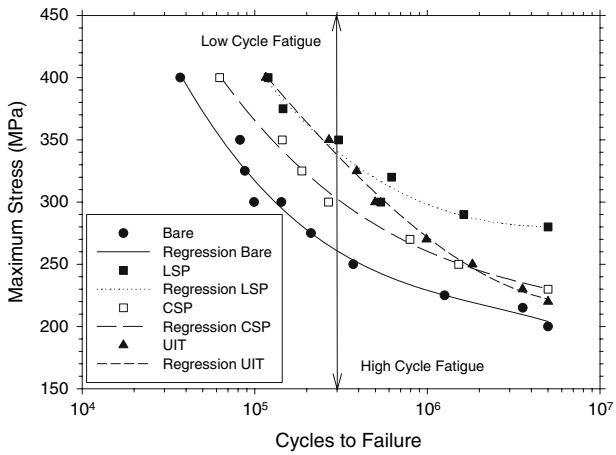

Fig. 4 *S-N* curves for 2024-T351 and the three selected SETs. All data beyond the 5 million cycles mark represent run-outs. The 300 K cycles mark is considered the transition from low to high cycle fatigue (intersection of two Basquin type lines for the bare material)

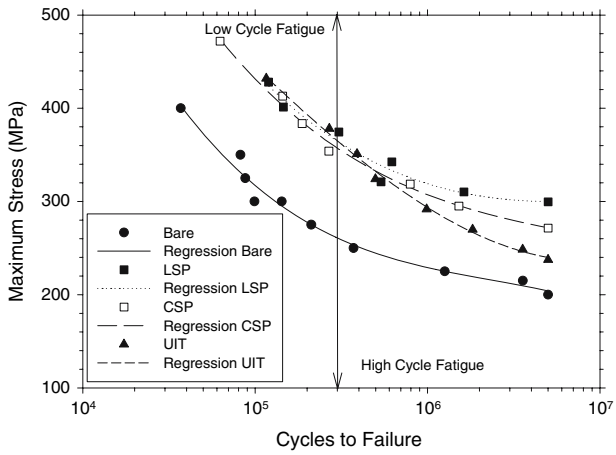

Fig. 5 Relative *S-N* curves according to data in Fig. 4

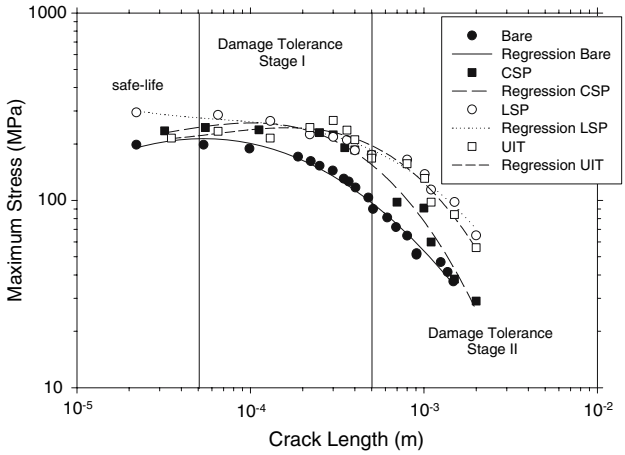

Fig. 6 Crack arrest curves for the three selected SETs at $R = 0.1$

(strong cold work). Surface roughness on the other hand, with most probable effect the acceleration of the propagation rate of short cracks, seems to produce minimum consequences. The improvement from CSP is uniform throughout the stress levels. The above indicate the potential of the material to simultaneously experience the effects of several SETs products and the fact that *S-N* curves are not representative of the true potential of SETs.

To tackle the above problem, a Kitagawa-Takahashi type of testing was adapted to reveal the effect of SETs on crack arrest. The method used for the determination the crack arrest behavior was repeated $\Delta\sigma$-shedding. The test procedure follows the ASTM recommendation (Ref 13). Deviation from the above was that the crack was allowed to initiate naturally at a stress level of 10% above the fatigue limit. In the case where secondary cracks were believed to interfere with the propagation of the main crack, the test was repeated. Crack monitoring was performed using a video camera mounted on an optical microscope and a dedicated image-capturing card supported by a high-end computer. Crack measurement was performed using image analysis software (SigmaScan by SPSS). The software is based on the tracking of the crack using a mouse. To facilitate crack observation, the surface of the specimens was polished using a succession of finer grade emery papers until attenuation of roughness at approximately Ra ~0.8 μm. Low rotational speed and water cooling was selected on the circular polisher to minimize the relaxation of residual stresses due to heating. To identify such fine loss of thickness, a high accuracy chemical scale was used. In the case of CSP, the removed surface was calculated at 1.6 μm. The results are shown in Fig. 6.

The results indicate that the effect of SETs on the crack arrest ability of 2024-T351 is twofold. For safe-life approach where the crack arrest capacity is examined against possible intrinsic crack like defects and the quality of microstructure (usually examined within size comparable to that of the average grain) the results indicate that except from LSP the other SETs caused minimum increase (considering a safety factor of 1.2 to encounter for possible scatter). In the area of damage tolerance—Stage I (Such region provides information in relation to the detection accuracy of most non-destructive inspection methods and is useful for the provision of detection probability functions. The region is also critical for designing against multiple-site damage, foreign object damage, etc.) the UIT showed maximum performance followed by the LSP and CSP. This is due to its induced residual stress profile. In the region denoted damage tolerance—Stage II (region where long crack propagation behavior and residual strength is of primal importance), it was shown that only LSP and the UIT can be held responsible for increasing the threshold value for crack propagation. The effect of CSP exhibited performance similar to that of the bare material. A rational explanation could be sought in the inability of CSP to establish residual stresses at such depths. In addition is should be noted that the crack arrest performance of CSP in this region does not follow the −0.5 gradient needed to establish a stress intensity factor nature.

Residual stresses are likely to relax especially under the application of external stresses (Ref 10). The rate and mechanism of their relaxation is complex and still eludes the academic community. Except from the effect of stress level, stress ratio effects, residual stress profile, relaxation ahead and behind the crack tip and the effects associated with the elastic anisotropy of the material are some of the parameters which will dominate research in the area for the years to come. Considering the elastic nature of the residual stresses and their ability to prolong the transition from local to global yielding (they cannot change global yielding values and neither other elasto-plastic properties), the time needed to detect a crack of particular length could provide vital information. In Fig. 7, the time needed (cycles) to detect a 70 μm and 1 mm crack at three different stress levels is presented. The crack lengths have been chosen in order to examine the effect of cold work (70 μm) and residual stress 1 mm.

The results indicate that for both crack lengths and all stress levels SETs caused a significant increase in the detection time. For the 70 μm crack, prolongation of detection time seems to decrease with lowering the stress level indicating the significance of cold work at high stress levels, where significant relaxation of the residual stress is expected. In contrast, the number of cycles needed to detect a 1 mm crack seems to gradually increase with stress reduction indicating the significance of the residual stresses and cold work. Herein, the slightly better performance from the UIT is due to the deeper residual stress profile. The selected stress levels and overall performance from the LSP prohibit similar comparison.

4. Discussion and Conclusions

The work indicates that the three selected SETs can increase the fatigue resistance of the 2024-T351 aluminum alloy. Yet, each treatment can endorse different degrees of improvement associated with specific design requirements. LSP covers every aspect of design requirements from safe-life to damage tolerance. CSP is likely to be used in cases where safe-life approach is been used. Its narrow depth of residual stresses can only endorsed improvement in the damage tolerance—stage I region. UIT exhibits better performance in the damage tolerance—stage II region taking advantage of its deep residual stress profile.

In the experimental section, it is indicated that traditional evaluation procedures used for residual stress free material are not necessarily applicable in the examination of SETs. For example, crack arrest testing in the case of CSP showed a strong deviation from a gradient denoting linear elastic fracture

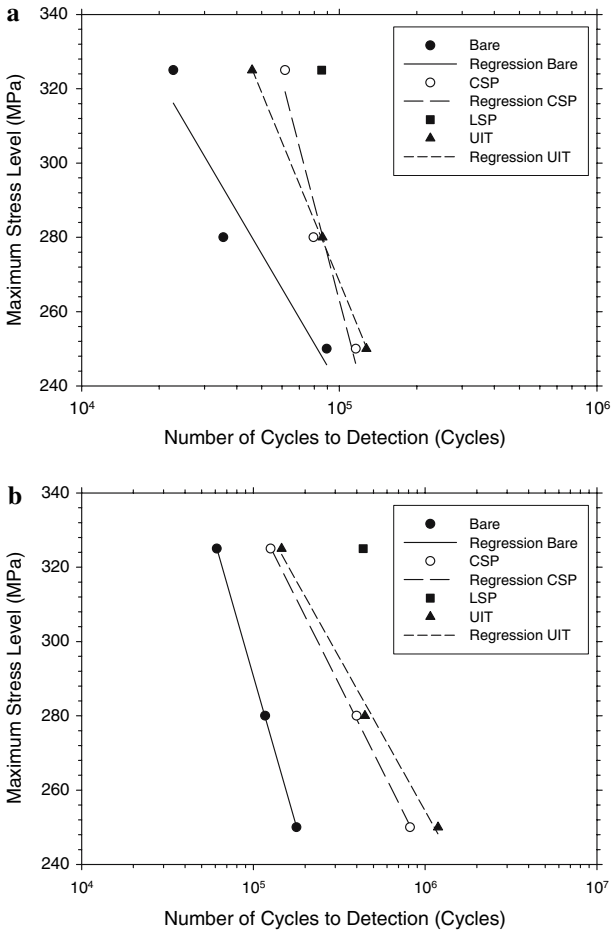

Fig. 7 Number of cycles required to detect a crack of (a) 70 μm and (b) 1 mm as a function of stress level

mechanics and hence such material property cannot be established.

There are several unanswered questions, which require further examination. Throughout the paper the similitude concept and hence the use of the stress intensity factor has been avoided. This is because; the stress and time dependent nature of the residual stresses is likely to compromise such representation. In addition, whether the residual stresses and cold work are likely to affect the crack shape (by affecting the aspect ratio of the crack) is still unknown and strongly depends on the specimen design, testing conditions, etc.

Except of the LSP which proven itself throughout every aspect of the testing matrix, its use especially in large aerospace components (skin, stringers, etc) is rather prohibited due to cost. CSP being the most inexpensive can be used as an extra safety factor in designs where the crack is unlikely to pass damage tolerance—stage I region undetected. Of course CSP is strongly affected by quality control issues especially in ensuring the uniform distribution of its surface roughness. The UIT on the other hand provides improvement throughout the damage tolerance—stages I and II region similar to that of the LSP.

The fact that LSP over performed the CSP and UIT, both in the high and low cycle fatigue region, remains an unanswered question specifically since the treatment does not benefit from cold work. A possible but still unproven explanation lies within the fact that the material itself exhibits significant cyclic hardening with values of cyclic yield stress approaching that of the ultimate tensile strength (behavior which indicates the small potential for improving fatigue resistance through cold work). Annealing to remove the residual stresses and hence examining only the effect of cold work is unworkable in the case of this alloy due to potential overaging effects.

References

1. J.Z. Gronostajski and J.R. Garstka, Explosive Hardening of Aluminium Alloys, *Sheet Metal Industries*, 1983, **60**(7), p 418–421
2. I. Altenberger, Alternative Mechanical Surface Treatments: Microstructures Residual Stresses and Fatigue Behaviour, *Shot Peening-ICSP8*, L. Wagner, Ed., Willey-VCH, 2003, p 421–434
3. J.W. Park, J.W. Kim, and Y.H. Chung, Grain Refinement of Steel Plate by Continuous Equal-channel Angular Process, *Scripta Mater.*, Vol. 51, 2004, p 181–184
4. Y. Satio, H. Utsunomiya, N.T. Suji, and T. Sakai, Novel Ultra-high Straining Process for Bulk Materials—Development of the Accumulative Roll-bonding (ARB) Process, *Acta Mater.*, 1999, **47**(2), p 576–583
5. X. An, C.A. Rodopoulos, E.S. Statnikov, V.N. Vitazev, and O.V. Korolkov, A study of the Surface Nano-Crystallisation Induced by the Esonix Ultrasonic Impact Treatment on the Near-Surface of 2024-T351 Aluminium Alloy, *J. Mater. Eng. Perf.*, 2006, **15**(3), p 355–364
6. P. Krull, T. Nitcschke-Pagel, and H. Wohlfahrt, Influence of Shot Peening and High Pressure Water Peening on Near Surface Microstructure of 316 Ti Stainless Steel, *Surface Treatments IV*, C.A. Brebbia, J.M. Kenny, Eds., WIT Press, 1999, p 291–300
7. U. Martin, U. Altenberger, B. Scholtes, K. Kremmer, and H. Oettel, Cyclic Deformation and Near Surface Microstructures of Normalized Shot Peened Steel SAE 10451, *Mater. Sci. Eng.*, 1998, **A246**, p 69–80
8. C A. E R. Rodopoulos los Rios, Theoretical Analysis on Short Fatigue Cracks, *Int. J. Fatigue*, 2002, **24**, p 719–724
9. L Wagner, Mechanical Surface Treatments on Titanium, Aluminium and Magnesium Alloys, *Mater. Sci. Eng.*, 1999, **A263**, p 210–216
10. C A Rodopoulos, S.A. Crtis, E.R los Rios, and J.S. Romero, Optimisation of the Fatigue Resistance of 2024-T351 Aluminium Alloys by Controlled Shot Peening—Methodology, Results and Analysis, *Int. J. Fatigue*, 2004, **26**, p 849–856
11. C.A. J.S. S.A Rodopoulos Romero Curtis, E.R. los Rios, and P. Peyre, The Effect of Controlled Shot Peening and Laser Shock Peening on the Fatigue Performance of 2024–T351 Aluminium Alloy, *J. Mater. Eng. Perf.*, 2003, **12**(4), p 414–419
12. J.K. Li, Y. Mei, W. Duo, W. Renzhi, Analysis of Stress Concentrations Caused by Shot Peening and its Application in Predicting Fatigue Strength, *Fatig. Fract. Engng. Mater. Struct.*, **15**(12), 1992, p 1271–1279
13. R.C. McClung, Analysis of Fatigue Crack Closure During Simulated Threshold Testing, *Fatigue Crack Growth Thresholds, Endurance Limit, Design*, ASTM STP 1372, J.C. Newman, R.S. Piasik, Ed., ASTM, PA, 2000